

M31's Heavy Element Distribution and Outer Disk

Guy Worthey, Aubrey España

Program in Astronomy, Washington State University, Pullman, WA 99164-2814

Lauren A. MacArthur

*Department of Physics and Astronomy, University of British Columbia, Vancouver, BC
V6T 1Z1*

Stéphane Courteau

Department of Physics, Queen's University, Kingston, ON K7L 3N6

ABSTRACT

Hubble Space Telescope imaging of 11 fields in M31 were reduced to color-magnitude diagrams. The fields were chosen to sample all galactocentric radii to 50 kpc (≈ 9 disk scale lengths, or $>99.9\%$ of the total light enclosed). Assuming that the bulk of the sampled stellar populations are older than a few Gyr, the colors of the red giants map to an abundance distribution with errors of order 0.1 dex in abundance. The radially sampled abundance distributions are all about the same width, but show a mild abundance gradient that flattens outside ~ 20 kpc. The various distributions were weighted and summed with the aid of new surface brightness profile fits to obtain an abundance distribution representative of the entirety of M31. Since we expect M31 to have retained most of its congenital gas and subsequently accreted material, and since the present day gas mass fraction is around 2%, it must be a system near chemical maturity. This “observed closed box” is compared to analytical closed box models.

M31 suffers from a lack of metal-poor stars *and* metal-rich stars relative to the simplest closed-box model in the same way as the solar neighborhood. Comparing to several simple chemical evolution models, neither complete mixing of gas at all times nor zero mixing, inhomogeneous models give the most convincing match to the data. As noted elsewhere, the outer disk of M31 is a factor of ten more metal-rich than the Milky Way halo, ten times more metal-rich than the dwarf spheroidals cospatial with it, and more metal-rich than most of the globular clusters at the same galactocentric radius. Difficulties of interpretation are greatly eased if we posit that the M31 disk dominates over the halo at all radii out to 50 kpc. In fact, scaling from current density models of the Milky Way,

one should not expect to see halo stars dominating over disk stars until beyond our 50 kpc limit. A corollary conclusion is that most published studies of the M31 “halo” are actually studies of its disk.

Subject headings: galaxies: chemical evolution — stars: abundances — stars: giant — galaxies: individual: NGC 224

1. Introduction

Posters of the beautiful Andromeda galaxy (M31; NGC 224) and its elliptical companions M32 (NGC 221) and NGC 205 adorn many of our office walls, and we have knowledge of this nearby spiral that rivals and in some ways surpasses our knowledge of the Milky Way. In particular, the Andromeda galaxy promises to test theories of galaxy development and history that were concocted to explain observations in the Milky Way, that is, the modern versions of the Eggen, Lynden-Bell, & Sandage (1962) gaseous collapse and the Searle & Zinn (1978) falling fragments.

The Andromeda Galaxy has about the same baryonic-plus-dark mass as the Milky Way (Evans et al. 2000; Gottesman, Hunter, & Boonyasait 2002) but twice the number of globular clusters. Gas phase material comprises 2% of the baryonic total in M31, but about twice this in the Milky Way (van den Bergh 2000). Further, the Milky Way is forming stars at a greater rate, with about a factor of 4 greater mass in ionised hydrogen. Most of the gas in M31 is concentrated in a 10-kpc “ring of fire” seen in molecular gas, atomic hydrogen, and dust, although OB associations appear throughout the disk. van der Kruit (1989) finds that the bulge of M31 contributes 25% of the total light while Milky Way’s bulge contributes more like 12%. (One should temper this result with the realization that the Milky Way emits more light per unit mass than does M31; in terms of mass the percentage contributions may be more nearly equal. Also, our own *I*-band bulge-disk decomposition discussed below yields a bulge contribution of 12%, not 25%.)

Globular cluster systems differ in the two galaxies despite having about the same number of clusters per unit mass (van den Bergh 2000). With a dividing line between metal poor and metal rich placed at $[\text{Fe}/\text{H}] = -1.0$, Milky Way metal rich globular clusters are somewhat concentrated toward the center of the galaxy, but they are not strongly disk-like in a spatial sense despite the fact that they are often referred to as “disk globulars”. M31 has more metal-rich globular clusters than the Milky Way, and a significant subset appear to have strongly disk-like kinematics (Morrison et al. 2004). As in the Milky Way, the metal rich M31 globular clusters lie preferentially toward the center of the galaxy, but unlike the Milky

Way, very metal-rich globulars (of nearly solar abundance) are also found quite far from the center.

Halo field stars in the Milky Way have an abundance distribution similar to that of the globular clusters spatially coresident there: with a peak at $[\text{Fe}/\text{H}] \sim -1.5$ and a broad dispersion that matches the simplest of chemical evolution models, the “Simple model,” that assumes a closed box, full mixing, instantaneous recycling, and a constant heavy element yield in every generation of stars. Halo field stars in M31, if they do indeed belong to a halo population, are quite different. Among other authors, Brown et al. (2003), Rich, Mighell, & Neill (1996), Durrell, Harris, & Pritchett (2004), and Grillmair et al. (1996) find from HST color-magnitude diagrams that almost all of the field stars in the outer regions of M31 are more metal-rich than 47 Tucanae (at $[\text{Fe}/\text{H}] \sim -0.8$), the prototypical metal-rich disk globular cluster, with mean abundances for the giants of $[\text{Fe}/\text{H}] \sim -0.5$. This is almost alarming: why should a galaxy of about the same mass have a halo abundance a factor of ten higher?

The aforementioned “Simple Model” of chemical evolution is a “straw man” (easily knocked down) model that applies to a closed box of gas that turns into stars. However, its simplicity, along with the relative complexity of the alternative chemical evolution models, makes it a compelling starting point. Furthermore, taken as a whole, M31 inside a galactocentric radius of 50 kpc must be close to a closed box in that it does not seem reasonable that it *permanently* lost more than a pittance of its total gas mass to intergalactic space [models support this notion for high-mass galaxies in non-cluster environments, c.f. Governato et al. (2004)]. Given that almost all of its gas is either still in the M31 disk (2% by mass) or has been turned into stars (98% by mass) then on a global level, M31 is a closed box, or close enough to a true closed volume that outflow should be negligible.

Infall in M31 could have occurred throughout its history, perhaps episodically where each episode goes nearly to chemical completion before the next wave, or perhaps steadily where the M31 gas fraction has been monotonically decreasing to its minimum at the present epoch. In the latter case, the Simple model might be expected to apply fairly well to the M31 closed box without modification. In the episodic case, one would have a situation usually termed inhomogeneous chemical evolution. In inhomogeneous chemical evolution, different patches of the galaxy mix only slightly or not at all or are allowed to mix only between enrichment episodes.

A final aspect of M31 that affects discussion of its formation and chemical evolution is the nature of its stellar halo. M31 does possess a system of globular clusters that is spatially and kinematically spheroidal, with a net rotation of only $80 \pm 20 \text{ km s}^{-1}$ (Huchra 1993). Racine (1991) finds a globular cluster surface density profile of R^{-2} in the range $6 < R(\text{kpc})$

< 22 , but a steeper drop off, or even a cutoff, beyond this range. van den Bergh (1969) finds that the most metal-rich globular clusters all have velocities of $\pm 100 \text{ km s}^{-1}$ from the projected disk velocity at their locations, indicating a more disk-like motion for the metal-rich end of the cluster population. More extensive data (Morrison et al. 2004) indicates a significant fraction of M31 globular clusters have thin-disk kinematics, are sprinkled over the entire projected disk, and have abundances that span the entire metallicity range. The M31 globular clusters have a spread of integrated colors that covers about the same abundance range as Milky Way globular clusters, but contains a more equal number of clusters in each metallicity bin (Reed et al. 1994).

Field stars in the outer portions of M31 follow, at least roughly, an exponential $R^{1/4}$ profile (van den Bergh 2000). This is roughly $\rho(R) \propto R^{-5}$ in the outer regions, as opposed to R^{-3} as one would infer for globular clusters (Racine 1991). But the continuity of the inner and outer parts of the minor axis (illustrated, for example, in van den Bergh (2000), figure 3.7) do not demand a “halo” that is separate from an “outer disk”. In fact there is no evidence of a halo at all from the light profile of the galaxy. Support for this viewpoint can be found from the planetary nebulae kinematics of Hurley-Keller et al. (2004), who say, “If M31 has a non-rotating, pressure-supported halo, we have yet to find it, and it must be a very minor component of the galaxy.”

In following sections we discuss HST photometric observations that sample the whole range galactocentric radii within M31, then we present the inferred abundance distributions. (What we refer to as abundance distributions are called by many “MDFs,” or metallicity distribution functions, and are simply the fractions of stellar mass observed over the range of abundance.) The observed distributions are then weighted and summed to simulate a globally integrated “closed box” M31 abundance distribution, which is then compared to solar neighborhood observations and model predictions. We conclude with a discussion of the constraints imposed upon the chemical evolution and formation of the Andromeda galaxy.

2. Observations and Analysis

A number of archived HST images were selected from the “planned and completed exposures” list. The first selection pass was simply by coordinates and whether the exposure was an image. The next step was to look at whether exposure times were fairly long, and if images were taken through two filters. For the outer fields it was clear that only the WFPC2 had a wide enough field of view for counting enough stars for meaningful results. The inner parts of M31 were observed by many programs, so we sampled from those, ensuring that we covered the range of radii. Some fields we rejected late in the process. Inner fields suffer

from crowding, so only the PC chip was used. Outer fields suffer from sparse star counts, so all available chips were utilised.

The final fields are listed in Table 1 and illustrated in Figure 1. The table lists (1) a project-internal label for each field, (2) the WFPC2 filters used, (3) the semi-major axis in arcsec from our radially-dependent elliptical isophotal fitting, (4) the resultant galactocentric radius assuming an inclined circular disk in kpc, (5) the galactocentric radius in the plane of the sky (impact parameter) in kpc, (6) the original HST proposal number, (7) the weighting factor used for combining the different samples to make a composite M31 abundance distribution, (8) the number of stars counted above the color-dependent cutoff magnitude, and the abundance median (9) and FWHM (10). Many of these quantities are discussed below. The HST frames were pipeline processed for basic flat fielding and photometric calibration. Each data set consisted of some number of frames in two filters to be coadded or “drizzled” to make final frames. Some of the outer fields contained additional position shifts. In these cases, each position was reduced separately. DAOPHOT (Stetson 1987) was used to derive fluxes for as many stars as possible in each frame. Zero point and aperture corrections were applied. The fluxes were corrected for charge transfer efficiency effects via Whitmore et al. (1999) and transformed to Johnson-Cousins V and I via Holtzman et al. (1995). A reddening of $E(B - V) = 0.06$ mag (Schlegel, Finkbeiner, & Davis 1998) was assumed for all fields.

Once color-magnitude diagrams are constructed, it is a straightforward matter to overlay giant branches from isochrones of different abundances. Stars that lie between isochrone giant branches are assigned an abundance given by the mean of the flanking isochrones and binned. A faint cutoff given by $M_I - 0.25(V - I) = -2.40$ was applied so that photometric errors would not artificially broaden the inferred abundance distribution too much. Finally, a correction for RGB stellar lifetimes was applied to transform the observed star counts to mass fractions (assuming an initial mass function for low-mass stars that is constant as a function of heavy element abundance). More discussion can be found in Grillmair et al. (1996) and Worthey et al. (2004) about the technique. Despite the faint cutoff, residual photometric error does slightly increase with width of the resultant abundance distribution. We ignore this effect because it is quite difficult to correctly implement such a deconvolution given the geometry of the color-magnitude diagram and also because rough estimates indicate that, with the observed widths of roughly 0.6 dex for the final abundance distributions, the increase of width due to photometric errors is only a few percent.

A possible problem worth recapping is the question of age and age spreads. Age modulates giant star colors rather less than abundance in a logarithmic sense. The way Worthey (1994) puts it, the line of null color change is $d[\log(\text{age})]/d[\log(\text{abundance})] = -3/2$ so that

(for example) an age change from 8 Gyr to 10 Gyr can be exactly offset by an abundance change of $-2/3\log(10/8) = -0.06$ dex. If the underlying age spread is 9 ± 3 Gyr the corresponding abundance uncertainty is 0.08 dex. This error is slightly smaller than the one we infer from random photometric uncertainties (~ 0.1 dex). The best claim for intermediate-age subpopulations in the outer parts of M31 is that of Brown et al. (2003), but “intermediate age” for those authors is ≈ 6 Gyr. A subpopulation of this age is too old to cause any significant change in the abundance distribution inferred from giant colors.

3. Abundance Results

Figure 2 shows the resultant series of abundance distributions for the various pointings, except that the star-starved outer pointings have been summed. One can see a steady progression in median abundance that goes from metal-rich in the inner disk to relatively metal-poor in the outskirts. The widths of the distributions do not change much from center to edge, and are similar to the width of the abundance distribution in the solar neighborhood (FWHM widths are listed in Table 1, derived by averaging the top two bins to find the maximum, then linear interpolation for the half-widths).

Figure 3 shows the median abundances for each field, but split into median abundance for each chip (PC, WF1, WF2, or WF3) in the cases where multiple chips were reduced. This is in order to gauge the effects of counting statistics. The figure shows that the outer disk-halo abundance holds relatively steady at $[\text{Fe}/\text{H}] \approx -0.5$. Gas-phase abundances from HII regions are also plotted on the figure to show the present-day abundance. The nebular abundances at least roughly agree with the slope of the gradient in the inner 25 kpc. To the extent to which one can trust the nebular zero point, the gas is at an abundance roughly 0.2 dex higher than the median of the stars, which puts the gas on the high-abundance end of the stellar abundance distributions. This is what one would expect with Simple-model type chemical evolution with good mixing. With inhomogeneous chemical evolution, one would expect individual star formation regions to be distributed about the same way as the fossil stars. We do not emphasise this point because the nebular abundance zero point does have considerable uncertainty.

The galactocentric radii of Figure 3 come from new elliptical isophotal fits of an I band mosaic (Choi et al. 2002). The azimuthally-averaged surface brightness profile was extracted following the method of Courteau (1996) and decomposed into bulge and disk components. These are shown in Figure 4. The decomposition technique is fully described in MacArthur, Courteau, & Holtzman (2003). The surface brightness limit of the image was much too bright to include regions that could be considered halo regions. The sizes and orientations of

the fitted ellipses were used to generate the Table 1 semi major axis column. Then, assuming an inclined circular disk and a distance of 770 kpc (Freedman & Madore 1990), these semi major axis values were converted to a galactocentric radius, also listed in Table 1 and used for Figure 3.

The isophotal fit was extrapolated with an exponential surface brightness profile for the disk to estimate the total light of the galaxy. The observed cumulative light profile plus the extrapolation is shown in Figure 5. Locations of HST fields are also shown in this figure, including the inner fields (in08, in09, and in10) that were eventually dropped because stellar crowding made deriving a reliable abundance histogram impossible. The curve in Figure 5 was used to assign each pointing with a weight representing the fraction of the galaxy “covered” by the pointing. These weights are also listed in Table 1. One notices that field “In07” gets a lot of weight. This is because it is the innermost field that was not beset with overcrowding problems. This field lies outside the bulge. This means that the bulge, as such, is not sampled. The fitted ratio of total bulge light to total disk light is 0.137.

The weights for each field were then used to construct an all-M31 abundance distribution from the individual sampled distributions. This global abundance distribution should be a good approximation to the M31 closed box. The weighted-sum abundance distribution and each of the individual distributions are tabulated in Table 2 (except that the outer fields are averaged). The Table 2 distributions are normalised to integral one. The weighted sum distribution has full-width-half-maximum (FWHM) of about 0.69 dex, slightly broader than any of the individual abundance distributions. We compare this global abundance distribution to local observation and theory in the next section.

4. Basic Chemical Evolution Models and Comparisons

We can compare the global M31 abundance distribution to the solar neighborhood abundance distribution and also simplified models of chemical evolution. This section recaps the basics of chemical evolution and the two ends of the spectrum of mixing: the Simple model with perfect mixing, and an inhomogeneous model with zero mixing. We then compare to data, then try additional model variants.

4.1. Simple Model

The Simple model of chemical evolution assumes an isolated system, no infall or outflow, of one zone, whose total mass is constant. It begins as pure gas with with a metal abundance

of $Z = 0$ and is well mixed at all times. In addition, the IMF and nucleosynthetic yields of the primary elements in the stars remains constant.

To develop the Simple model [c.f. Searle & Sargent (1972); Audouze & Tinsley (1976); Binney & Tremaine (1987)], we define M_h as the mass in gas phase made of heavy elements, M_g the mass of the gas, M_s the mass in stars and define the abundance, or, loosely, the metallicity, Z as

$$Z = \frac{M_h}{M_g} \quad (1)$$

If an incremental parcel of new stars is formed and only δM_s remains locked in the stars, then the rest must be returned. The amount of gas returned by newly formed stars in heavy elements is $p\delta M_s$, where p is the “nucleosynthetic yield” in a given generation of stars. One could assume that p is a function of time or metallicity, but the Simple model assumes a constant yield. We can now calculate the change in the amount of metal-rich gas, which is the gas returned minus the gas which formed the stars:

$$\delta M_h = p \delta M_s - Z\delta M_s = (p - Z)\delta M_s \quad (2)$$

Meanwhile, the change in the gas metallicity is as follows:

$$\delta Z = \delta\left(\frac{M_h}{M_g}\right) = \frac{\delta M_h}{M_g} - \frac{M_h}{M_g^2}\delta M_g = \frac{1}{M_g}(\delta M_h - Z\delta M_g) \quad (3)$$

By combining equations (2) and (3) and using the fact that mass is conserved such that $\delta M_s = -\delta M_g$, we obtain

$$\delta Z = \frac{1}{M_g}[(p - Z)\delta M_s - Z\delta M_g] = \frac{1}{M_g}[(-p + Z - Z)\delta M_g] = -p \frac{\delta M_g}{M_g} \quad (4)$$

If the yield p is not a function of time, integration gives

$$Z(t) = -p \ln \left[\frac{M_g(t)}{M_g(0)} \right] \quad (5)$$

This expression for Z is a function only of the yield and the gas fraction, hence the term “Simple” for this scheme. Let us rework this formula to give us what we observe: the number of stars at each metallicity. If we let the gas fraction approach chemical completion, how many stars of what metallicity do we expect? The mass in stars of Z less than $Z(t)$ at some time t is

$$M_s[< Z(t)] = M_g(0) - M_g(t) = M_g(0) \left[1 - \exp\left(\frac{-Z(t)}{p}\right) \right] \quad (6)$$

so the differential fraction of mass at each Z is

$$\frac{dM_s}{dZ} = \frac{\exp(-Z/p)}{p} \quad (7)$$

But abundance is typically measured in terms of the logarithmic number abundance like, for example, $[\text{Fe}/\text{H}]$, or $[\text{M}/\text{H}]$ if one lumps all heavy elements together. We would like to recast equation (7) by defining $F \approx [\text{M}/\text{H}]$, where $F = \log(Z/Z_\odot)$. (Note that this is not precisely correct. If “heavy” elements are those that are not hydrogen or helium, then one should account for the fact that very metal-rich stars deplete their light elements and define $F = \log \frac{Z/(1-Z)}{Z_\odot/(1-Z_\odot)}$. However, if one considers stars from very metal-poor to a few times the solar abundance of $Z_\odot \approx 0.02$, one can safely stick to the approximate form.) Using $Z = Z_\odot 10^F$ and $dZ = Z dF/\log(e)$, we arrive at the less-than-elegant expression

$$dM = \frac{Z_\odot 10^F}{p \log(e)} \exp \left[-\frac{Z_\odot}{p} 10^F \right] dF \quad (8)$$

This distribution should be truncated at the gas fraction appropriate for the system. In the case of M31, the present day gas fraction is $\frac{M_g(t)}{M_g(0)} = 0.02$.

4.2. Inhomogeneous Enrichment Models

Suppose that, in a cube of gas, enrichment occurs in patches scattered throughout the cube. These patches may or may not overlap spatially, so that if little mixing occurs then a variety of abundances will coexist in the gas. Such a picture is called inhomogeneous chemical evolution, and has been studied in several works [e.g. Tinsley (1975), Searle (1977), and Malinie et al. (1993)]. We compare our M31 composite abundance distribution to a model with zero mixing (Oey 2000). This model has five parameters, the volume filling fraction Q of the enriched bubbles, the number n of enrichment generations, the mean a and standard deviation σ of the abundance distribution typical of a collection of local star formation events, and the present day gas fraction $\mu = M_g(t)/M_g(0)$. Unlike Oey (2000), we assume that each generation of star formation is described by a Gaussian abundance distribution, i.e., we stop at Oey’s equation (8) rather than going on through equation (13).

4.3. Some Comparisons

Figures 6, 7, 8, and 9 show various data-model inter-comparisons. In Figure 6 the Simple model and the global-M31 abundance distribution are compared. Note that M31’s small present-day gas fraction means that chemical evolution in the Simple model is almost complete, and only a small modification in the most metal-rich bin is needed to account for the truncation of the model distribution. What is evident immediately is that the Simple model abundance distribution is wider, with an extended tail toward metal-poor stars. This

is the same mismatch that is seen in the solar neighborhood and is termed the G dwarf problem.

In Figure 7 a Simple model (with a yield 0.1 dex higher than 6) is compared to various solar neighborhood data sets. The broadest of these is Wyse & Gilmore (1995) (FWHM 0.75 dex), and the narrowest is Jørgensen (2000) (FWHM 0.47 dex). These widths completely bracket our derived M31 abundance distribution widths listed in Table 1 and the closed-box M31, which has a FWHM of 0.69 dex. The Haywood (2001) distribution is intermediate in width (FWHM 0.61 dex), but is shifted toward metal-rich stars. The Wyse & Gilmore (1995) paper emphasised corrections to augment the metal-poor end of the distribution to account for thick disk and halo stars while the Haywood (2001) paper emphasised selection effects against metal-rich stars. The differences between authors is large, and illustrates that the solar neighborhood data are subject to a fair amount of interpretation. All of the distributions, however, are more narrow than the Simple model (FWHM 0.87 dex), so the solar neighborhood has a G dwarf problem for all data sets.

Some Oey (2000) models are plotted in Figure 8, with parameters listed in the figure itself. The broad model (FWHM 0.76 dex) with $n = 400$ and $Q = 0.8$ is similar to what is plotted in her Figure 4 that is meant to match the solar neighborhood data, although Oey uses a different gas fraction and a non-Gaussian abundance distribution from individual star forming events. The other, narrower distribution (FWHM 0.55 dex) has the number of events multiplied by the volume filling factor of order one ($nQ \sim 1$). So this narrow model that comes close to fitting the observations is a virtually one-shot self-enrichment event with the abundance distribution of one star formation generation nearly equal to the observed M31 distribution. The narrow model also uses up nearly all the available gas after only one generation, a prospect unlikely enough that this corner of parameter space in the Oey model is probably rejectable. In summary, although inhomogeneous chemical evolution must operate at some level in real galaxies, the pure, zero-mixing case as applied in the Oey models does not perfectly match M31 without tuning the parameters in unlikely ways.

4.4. Modified Simple Model

Any number of modifications to the Simple model can make it fit the data better. We modify the Simple model to have a yield that starts high and decreases with increasing Z as $p = \frac{p_0}{Z+c}$. We have not seen this particular variant in the literature; we call it the “rational decreasing yield model”. This version is then a three-parameter model with the gas fraction remaining as the primary parameter, but the yield now parameterised with p_0 and ϵ . Substituted into equation (4) and integrated, the expression for p yields a quadratic

with positive root

$$Z(t) = -\epsilon + (\epsilon^2 - 2p_0 \ln \left[\frac{M_g(t)}{M_g(0)} \right])^{1/2} \quad (9)$$

The analog of equation (6) for this model is

$$M_s[< Z(t)] = M_g(0) \left(1 - \exp \left[-\frac{(Z + \epsilon)^2 - \epsilon^2}{2p_0} \right] \right) \quad (10)$$

The analog of equation (7) is

$$\frac{dM_s}{dZ} = \frac{Z + \epsilon}{p_0} \exp \left[-\frac{(Z + \epsilon)^2 + \epsilon^2}{2p_0} \right] \quad (11)$$

And converting to ten-based logarithmic units yields

$$dM_s = \frac{Z_\odot 10^F + \epsilon}{p_0} \exp \left[-\frac{(Z_\odot 10^F + \epsilon)^2 - \epsilon^2}{2p_0} \right] \frac{Z_\odot 10^F}{\log(e)} dF \quad (12)$$

Figure 9 illustrates the dramatic improvement in fit that can be achieved with a variable yield. The parameter p_0 controls the abundance of the peak of the distribution, while ϵ controls the width. The scale on the y axis and the thin decreasing line represent the variable yield, computed with $p_0 = 0.00019$ and $\epsilon = 0.004$. The shape of the resultant abundance distribution is not sensitive to modest changes in the parameters; a good feature of this modified model. Another good feature is the plateau at the very metal-poor end, but there are mild mismatches at various points as well. The width is $\text{FWHM} = 0.62$ dex.

There is astrophysical support for a yield that decreases with increasing metallicity. Worthey, Dorman, & Jones (1996) note that, so far, every galaxy studied that is bigger than M32 seems to suffer a “G dwarf problem” of having a narrow abundance distribution compared to the Simple model. This argues for a universal phenomenon rather than a special case scenario, and having a top-heavy initial mass function (IMF) for metal-poor stellar populations is the most obvious way to have a yield that decreases with time or abundance. Bresolin, Kennicutt, & Garnett (1999) find that star forming regions of greater than solar abundance appear to have a smaller upper IMF mass limit, a result that we find very suggestive, as it applies to the metal-rich end of the abundance range. At the metal-poor end, Cen (2003a,b) finds that Wilkinson Microwave Anisotropy Probe observations of early-universe reionization are much easier to match if the first generations of stars had a top-heavy IMF. Scannapieco, Schneider, & Ferrara (2003) find some evidence from chemical yields that Population III stars are likely to be very massive, and Schneider et al. (2002) point out that studies of metal-free gas collapse and fragmentation predict very massive Population III stars, but also that most such massive stars should turn into black holes so

that only in the mass range $140M_{\odot} < M < 260M_{\odot}$ can pair-production supernovae drive effective element dispersal. Our scheme for connecting the endpoints with a rational function is, of course, artificial, but its easy success is enlightening.

4.5. Malinie et al. (1993)

Finally, we also compare to an inhomogeneous chemical evolution model in which mixing is allowed between inhomogeneous mixing events, the model of Malinie et al. (1993). This model was built to emulate the solar neighborhood situation and, like the Oey model, has 5 parameters; the number of mixing events N , the fraction of gas consumed in each event f , an initial metallicity Z_0 , a metallicity dispersion δZ , and a yield y . Figure 9 illustrates the match of the Malinie et al. (1993) model (dashed line) if the initial metallicity $Z_0 = 0$ and the fraction of gas consumed in each event (f) is set so that the final gas fraction is 0.02 instead of 0.2 as in their paper. Other parameters are left as in Malinie et al. (1993) ($N = 100$, $\delta Z = 0.01$, and $y = 0.72Z_{\odot}$). Setting the number of events N equal to 100 implies that there was quite a lot of mixing in the history of M31. The Malinie model (FWHM 0.63 dex) is quite successful at roughly matching the M31 closed-box abundance distribution (FWHM 0.69). The only parameter changes from the Milky Way case were those that one could expect: an adjustment for a lower gas fraction in M31 and an initial metallicity of zero that is appropriate for a closed box situation.

5. Discussion

In summary, the comparisons of the observed M31 closed box abundance distribution with chemical evolution models showed that (1) the Simple model is too broad, (2) the 5-parameter inhomogeneous zero-mixing models that we tried were either too broad or in physically questionable corners of parameter space, (3) a modified Simple model with 3 parameters instead of two with a yield that decreases with abundance fits the M31 closed box abundance distribution fairly nicely, and (4) a 5-parameter inhomogeneous model that allows mixing between enrichment events (100 of them assumed) also fits very well with sensible changes in input parameters. There can be no definitive quantitative conclusion since we did not try every model that exists, but these results suggest that the gas from which M31 formed was mixed fairly thoroughly during chemical evolution.

Combined with the result of Worthey, Dorman, & Jones (1996) that elliptical (i.e. spheroid-dominated) galaxies also have a narrow abundance distribution compared to the

Simple model, the “narrowness” of the abundance distribution appears to be a universal phenomenon in all large galaxies, not just for disk galaxies. This is circumstantial evidence that the abundance distribution is generically narrower than the Simple model suggests. Since outflow is ruled out for closed boxes, the remaining classical solutions to this problem (Audouze & Tinsley 1976) are (1) prompt initial enrichment, (2) infall without outflow, (3) dropping the assumption of instantaneous recycling, i.e. allowing for time-delayed yields and allowing inhomogeneous enrichment. Our Z -dependent yield is an implementation of (1), and it works fairly well except that the parameterisation is not physical. Scheme (2), infall, we did not explore, but we expect that it could be made to produce a narrow abundance distribution with suitable tuning of yield, mixing, and infall parameters, especially if it started with a chemical evolution scheme that produces a narrow abundance distribution in the closed-box case. The major caveat with infall is that the parameters would have to be tuned about the same way for ellipticals as well as spirals since they have very similar abundance distributions, but we know the formation time scales for ellipticals are shorter than for spirals. Furthermore, processes like merging and harassment should also strongly alter infall assumptions and therefore should produce different abundance spreads in the end.

Scheme (3) was partially explored with inhomogeneous models, with some good matches, but the easiest matches were those that included some mixing of gas during chemical evolution. Delayed injection of heavy elements serves to add metal-poor stars to the system, and so would make the fit worse if it were included. We are therefore left with a common theme for chemical evolution; that there is a uniqueness problem. Several, or many models with different assumptions can match the data quite well (Tosi 1988). The only conclusion we draw about chemical evolution, that some mixing seems to be indicated, is a weak conclusion that (1) could easily be destroyed by some zero-mixing inhomogeneous model that fits the M31 abundance distribution slightly better, but (2) must be true anyway since a zero mixing hypothesis has zero probability of being literally true.

As a prelude to further discussion, we ask “at what radius do we expect M31 halo stars to dominate over disk stars?” assuming that the M31 halo resembles that of the Milky Way. Disks are usually modelled with an exponential of the form $I = I_0 \exp(-R/h)$, where h is the scale length and I is a surface brightness, not a density. The Milky Way halo is found to follow a power law density $\rho = \rho_0 R^{-3.5}$ outside of 5 kpc (van den Bergh 2000). Provided we can trust these functional forms, an exponential will fade faster than a power law, so a halo will always dominate outside some radius.

To evaluate the surface density of the halo, normalised to the local surface density of the disk, we use the results of Sandage (1987), integrating his Table 1 kinematically derived densities as a function of height above the disk and adopting local density ratios for disk:thick

disk:halo of 500:30:1 (and for our purposes we simply subsume the thick disk into the disk). The problem is then fully specified except for the disk scale length h . Figure 10 shows the prediction for the V -band Milky Way scale length $h = 4.2$ kpc (van den Bergh 2000). Van den Bergh notes that estimates of 2 to 6 kpc for the Milky Way scale length h exist in the literature, part of this spread being a function of the wavelength studied. The Chen et al. (2001) models are also shown in Figure 10 exactly as integrated from the published density model (including a shallower halo density power law of -2.5 and disk scale length of $h = 2.25$ kpc). These results indicate that, in the Milky Way, halo stars become more common than disk stars at galactocentric radii of $35 < R < 45$.

The scale length of M31 is more secure than that of the Milky Way. van den Bergh (2000) quotes $h = 5.7$ kpc for the V band, and our own I band decomposition gives $h = 5.6$ kpc [or 5.7 kpc if the slightly longer distance of 784 kpc Stanek & Garnavich (1998) is used]. For a scale length of this size, and also doubling the density of the M31 halo because M31 has twice the number of globular clusters, Figure 10 indicates that we should *not* expect to see the halo dominate at any radius that we sample, and that halo stars should become relatively numerous only outside a radius of 50 kpc from the center of M31.

This should be slightly tempered by a geometrical consideration: If the halo is spherical, a line of sight intersects the halo at an impact parameter $R_h \approx D\theta$, where D is distance and θ is the angle between the line of sight and the M31 nucleus. The impact parameter is the same as the galactocentric radius in the inclined disk (R_d) only along the major axis of the isophote. For most lines of sight, the projected disk is foreshortened so that $R_h < R_d$, and the foreshortening is at a maximum along the minor axis of an isophote. For gauging this possible amplification effect, we list both radii in Table 1 [the amplification of the halo is roughly $(R_d/R_h)^{2.5}$ assuming the halo density profile is $\rho \propto R^{3.5}$]. We find that fields near the minor axis can have the halo boosted by a factor of order ten from this effect. Of course, if the halo is flattened instead of spherical (as the Milky Way's is believed to be) the boost rapidly diminishes. And there is evidence from globular clusters that the halo density falls off faster than $\rho \propto R^{-3.5}$ outside of 30 kpc Racine (1991). It is quite possible that, except for nearly edge-on spirals where projection effects dominate, the disk stars outnumber the halo stars at all radii.

If we are seeing disk stars in all fields, then explaining the relatively metal-rich mean abundance of $[\text{Fe}/\text{H}] \approx -0.5$ becomes quite natural compared to trying to explain why the halo of M31 is a factor of ten more metal-rich than the Milky Way halo. If we are seeing disk stars, then the M31 halo can be presumed to be alive and well and very similar to the Milky Way halo, which, after all, is supposed to compose less than 2% of the mass of the Galaxy. Alive and well, but, as yet, unseen.

Many authors have called the outer regions of M31 “halo,” but for the most part this is a term of convenience, and not indicative of true pressure-supported halo status since we are almost completely ignorant of the kinematics of these stars. It is interesting to wonder how interpretations change if disk status is assumed. Brown et al. (2003) find an “intermediate age” subpopulation in a field at 11 kpc galactocentric radius in the plane of the sky (we derive 13.6 kpc from the coordinates given in the paper plus our assumed distance), or 40.8 kpc galactocentric radius on the extrapolated M31 disk. If this is disk, then finding non-ancient stars seems perfectly fine, and the main issue might be why there are no younger stars present. Perhaps this is evidence that star formation in the outer M31 disk was quenched after about half a Hubble time.

By counting red giants in the vicinity of M31, Ferguson et al. (2002) established the presence of dynamical clumping or streaming at radii out to 55 kpc in an elliptical survey region shaped like an extrapolation of the disk. Some substructure detected strongly resembles merging events, but some of the features inside ~ 30 kpc also look like flocculent spiral structure. Companions M32 and NGC 205 project on the sky *inside* these structures. The parts of the Ferguson et al. (2002) Fig. 2 map outside ~ 30 kpc look rather uniform (except for the substructures) but this may be due to Galactic foreground stars (they were not subtracted). The Ferguson et al. (2002) maps certainly do not rule out that the outer parts of M31 are dominated by a disturbed and tidally shredded disk.

A speculative synthesis of these considerations might be that M31 formed a gaseous, well-mixed disk and a Milky Way-like halo in the first half of a Hubble time. Chemical enrichment proceeded in a “disky” way via rotational mixing, galactic fountains, and the occasional supernova wind. Over time, the gas supply ran short so the outer disk stopped forming stars. Additionally, the satellite galaxies, especially M32, began to make their dynamical presence felt, adding stellar streams and tidally disturbing the stars that were already present. More measurements of stellar kinematics in the outer disk of M31 are required to settle this question.

We thank P. Guhathakurta and P. I. Choi for providing M31 image mosaic data. P. B. Stetson provided both the DAOPHOT program and valuable advice. S. Oey provided feedback of inestimable worth. S. C. and L. A. M. acknowledge support from the National Science and Engineering Research Council of Canada. This work was supported by grant AR-08745.01-A from Space Telescope Science Institute.

REFERENCES

- Audouze, J., & Tinsley, B. M. 1976, *ARA&A*, 14, 43
- Binney, J., & Tremaine, S. 1987, *Galactic Dynamics*, (Princeton University Press: Princeton)
- Blair, W. P., Kirshner, R. P., & Chevalier, R. A. 1982, *ApJ*, 254, 50
- Bresolin, F., Kennicutt, R. C., Jr., & Garnett, D. R. 1999, *ApJ*, 510, 104
- Brown, T. M., Ferguson, H. C., Smith, E., Kimble, R. A., Sweigart, A. V., Renzini, A., Rich, R. M., & VandenBerg, D. A. 2003, *ApJ*, 592, L17
- Cen, R. 2003, *ApJ*, 591, 12
- Cen, R. 2003, *ApJ*, 591, L5
- Chen, B., Stoughton, C., Smith, A., Uomoto, A., Pier, J. R., Yanny, B., Ivezić, Z., York, D. G., Anderson, J. E., Annis, J., Brinkman, J., Csabai, I., Fukugita, M., Hindsley, R., Lupton, R., & Munn, J. A. 2001, *ApJ*, 553, 184
- Choi, P. I., Guhathakurta, P., & Johnston, K. V. 2002, *AJ*, 124, 310
- Courteau, S. 1996, *ApJS*, 103, 363
- Dennefeld, M., & Kunth, D. 1981, *AJ*, 86, 989
- Durrell, P. R., Harris, W. E., & Pritchett, C. J. 2004, *AJ*, 128, 260
- Eggen, O. J., Lynden-Bell, D., & Sandage, A. R. 1962, *ApJ*, 136, 748
- Evans, N. W., Wilkinson, M. I., Guhathakurta, P., Grebel, E. K., & Vogt, S. S. 2000, *ApJ*, 540, L9
- Ferguson, A. M. N., Irwin, M. J., Ibata, R. A., Lewis, G. F., & Tanvir, N. R. 2002, *AJ*, 124, 1452
- Freedman, W. L., & Madore, B. F. 1990, *ApJ*, 365, 186
- Gottesman, S. T., Hunter, J. H., & Boonyasait, V. 2002, *MNRAS*, 337, 34
- Governato, F., Mayer, L., Wadsley, J., Gardner, J. P., Willman, B., Hayashi, E., Quinn, T., Stadel, J., & Lake, G. 2004, *ApJ*, 607, 688

- Grillmair, C. J., Lauer, T. R., Worthey, G., Faber, S. M., Freedman, W. L., Madore, B. F., Ajhar, E. A., Baum, W. A., Holtzman, J. A., Lynds, C. R., O’Neil, E. J., Jr., & Stetson, P. B. 1996, *AJ*, 112, 1975
- Haywood, M. 2001, *MNRAS*, 325, 1365
- Hodge, P. W., & Kennicutt, R. C. 1982, *AJ*, 87, 264
- Holtzman, J. A., Burrows, C. J., Casertano, S., Hester, J. J., Trauger, J. T., Watson, A. M., & Worthey, G. 1995, *PASP*, 107, 1065
- Huchra, J. P., in *The Globular Cluster-Galaxy Connection* (ASP Conference Series Vol. 48), ed. G. H. Smith and J. P. Brodie, San Francisco: Astron. Soc. Pac., 420
- Hurley-Keller, D., Morrison, H. L., Harding, P., & Jacoby, G. 2004, *ApJ*, accepted; astro/ph 0408137
- Jørgensen, B. R. 2000, *A&A*, 363, 947
- Kotoneva, E., Flynn, c., Chiappini, C., & Matteucci, F. 2002, *MNRAS*, 336, 879
- MacArthur, L. A., Courteau, S., & Holtzman, J. A. 2003, *ApJ*, 582, 689
- Malinie, G., Hartmann, D. H., Clayton, D. D., & Mathews, G. J. 1993, *ApJ*, 413, 633
- Morrison, H. L., Harding, P., Perrett, K., & Hurley-Keller, D. 2004, *ApJ*, 603, 87
- Oey, M. S., 2000, *ApJ*, 542, L25
- Racine, R. 1991, *AJ*, 101, 865
- Reed, L. G., Harris, G. L. H., & Harris, W. E. 1994, *AJ*, 107, 555
- Rich, R. M., Mighell, K. J., & Neill, J. D. 1996, in *Formation of the Galactic Halo, Inside and Out* (ASP Conference Series, Vol 92) ed. H. Morrison & A. Sarajedini, 544
- Sandage, A. 1987, *AJ*, 93, 610
- Scannapieco, E., Schneider, R., & Ferrara, A. 2003, *ApJ*, 589, 35
- Schlegel, D. J., Finkbeiner, D. P., & Davis, M. 1998, *ApJ*, 500, 525
- Schneider, R., Ferrara, A., Natarajan, P., & Omukai, K. 2002, *ApJ*, 571, 30
- Searle, L., in *The Evolution of Galaxies and Stellar Populations*, ed. B. M. Tinsley & R. B. Larson (New Haven: Yale Univ. Obs.), 219

- Searle, L., & Sargent, W. L. W. 1972, *ApJ*, 173, 25
- Searle, L., & Zinn, R. 1978, *ApJ*, 225, 357
- Sil’chenko, O. K., Burenkov, A. N., & Vlasyuk, V. V. 1998, *A&A*, 337, 349
- Stanek, K. Z., & Garnavich, P. M. 1998, *ApJ*, 503, L131
- Stetson, P. B. 1987, *PASP*, 99, 191
- Tinsley, B. M. 1975, *ApJ*, 197, 159
- Tosi, M. 1988, *A&A*, 197, 33
- van den Bergh, S. 2000, *The Galaxies of the Local Group* (Cambridge: Cambridge University Press)
- van den Bergh, S. 1969, *ApJS*, 19, 145
- van der Kruit, P. C. 1989, in *The Milky Way as a Galaxy*, ed. G. Gilmore, I. R. King, and P. C. van der Kruit (Sauverny: Geneva Observatory), 331
- Whitmore, B., Heyer, I., & Casertano, S. 1999, *PASP*, 111, 1559
- Wyse, R. F. G., & Gilmore, G. 1995, *AJ*, 110, 2771
- Worthey, G. 1994, *ApJ*, 95, 107
- Worthey, G., Dorman, B., & Jones, L. A. 1996, *AJ*, 112, 948
- Worthey, G. 1998, *PASP*, 110, 888
- Worthey, G., Mateo, M., Alonso-García, J., & España, A. L. 2004, *PASP*, 116, 295
- Wyse, R. F. G., & Gilmore, G. 1995, *AJ*, 110, 2771

Table 1. Pointings

Internal Label	Filters	a_{isophote} (Arcseconds)	R_d^b (kpc)	R_h^c (kpc)	Original HST Proposal	Weight	Number of Stars Counted	$\langle[M/H]\rangle$	FWHM
Out03	F55,F814	8970	33.5	33.3	5464	0.02860 ^a	158	-0.43	0.57 ^a
Out04	F55,F814	13295	49.6	18.9	5112	0.02860 ^a	215	-0.46	0.57 ^a
Out05	F55,F814	8520	30.8	19.0	5420	0.02860 ^a	189	-0.46	0.57 ^a
In01	F55,F814	7270	27.1	23.2	6859	0.03012	356	-0.40	0.65
In02	F55,F814	5685	12	8.8	6734	0.05449	1008	-0.50	0.68
In03	F55,F814	4215	15.7	14.5	6671	0.09507	1336	-0.56	0.60
In04	F606,F814	2940	1.0	3.0	6664	0.10487	529	-0.29	0.63
In05	F55,F814	3510	13.1	4.4	5322	0.06051	323	-0.46	0.58
In06	F55,F814	3090	1.5	8.3	6859	0.05077	371	-0.18	0.58
In07	F606,F814	1050	3.9	2.6	5971	0.43257	550	-0.11	0.63
In11	F55,F814	1530	5.7	3.8	6431	0.14300	631	-0.24	0.58

^aAll three “out” fields were summed before being assigned this quantity.

^b R_d is the galactocentric radius assuming a circular inclined disk geometry and a distance of 0.77 Mpc.

^c R_h is the galactocentric radius in the plane of the sky, that is, appropriate for a spherical geometry.

Table 2. Abundance Distributions

[M/H]	Out	In01	In02	In03	In04	In05	In06	In07	In11	Sum
-2.15	0.000	0.005	0.005	0.000	0.000	0.000	0.000	0.000	0.003	0.001
-2.05	0.000	0.004	0.004	0.000	0.003	0.000	0.000	0.002	0.003	0.001
-1.95	0.000	0.002	0.006	0.000	0.006	0.000	0.000	0.000	0.003	0.001
-1.85	0.000	0.001	0.006	0.000	0.009	0.000	0.000	0.000	0.003	0.001
-1.75	0.000	0.002	0.005	0.002	0.009	0.000	0.000	0.000	0.003	0.001
-1.65	0.000	0.002	0.006	0.002	0.006	0.000	0.000	0.000	0.003	0.001
-1.55	0.004	0.002	0.002	0.000	0.003	0.003	0.000	0.003	0.002	0.001
-1.45	0.000	0.007	0.005	0.000	0.009	0.003	0.004	0.003	0.007	0.004
-1.35	0.003	0.003	0.004	0.000	0.021	0.000	0.004	0.000	0.007	0.004
-1.25	0.003	0.004	0.010	0.000	0.015	0.000	0.000	0.002	0.008	0.003
-1.15	0.005	0.017	0.021	0.004	0.009	0.003	0.002	0.012	0.014	0.007
-1.05	0.010	0.014	0.025	0.006	0.013	0.006	0.002	0.010	0.016	0.008
-0.95	0.015	0.023	0.039	0.014	0.020	0.015	0.002	0.011	0.023	0.012
-0.85	0.023	0.035	0.051	0.019	0.027	0.000	0.002	0.016	0.048	0.016
-0.75	0.046	0.085	0.067	0.044	0.037	0.022	0.009	0.028	0.054	0.030
-0.65	0.096	0.107	0.119	0.054	0.064	0.019	0.017	0.049	0.092	0.047
-0.55	0.105	0.116	0.118	0.069	0.082	0.034	0.030	0.046	0.134	0.058
-0.45	0.119	0.143	0.124	0.087	0.124	0.068	0.072	0.081	0.120	0.089
-0.35	0.179	0.152	0.128	0.118	0.133	0.124	0.092	0.111	0.141	0.112
-0.25	0.180	0.119	0.099	0.151	0.133	0.121	0.098	0.111	0.123	0.113
-0.15	0.146	0.093	0.078	0.136	0.130	0.135	0.123	0.122	0.074	0.119
-0.05	0.047	0.047	0.052	0.154	0.094	0.117	0.144	0.112	0.049	0.116
0.05	0.019	0.014	0.021	0.117	0.041	0.200	0.196	0.168	0.045	0.138
0.15	0.002	0.004	0.003	0.018	0.010	0.089	0.110	0.077	0.010	0.066
0.25	0.000	0.001	0.001	0.004	0.002	0.029	0.052	0.026	0.008	0.029
0.35	0.000	0.000	0.000	0.001	0.000	0.006	0.026	0.008	0.004	0.013
0.45	0.000	0.001	0.000	0.000	0.002	0.006	0.014	0.004	0.004	0.007

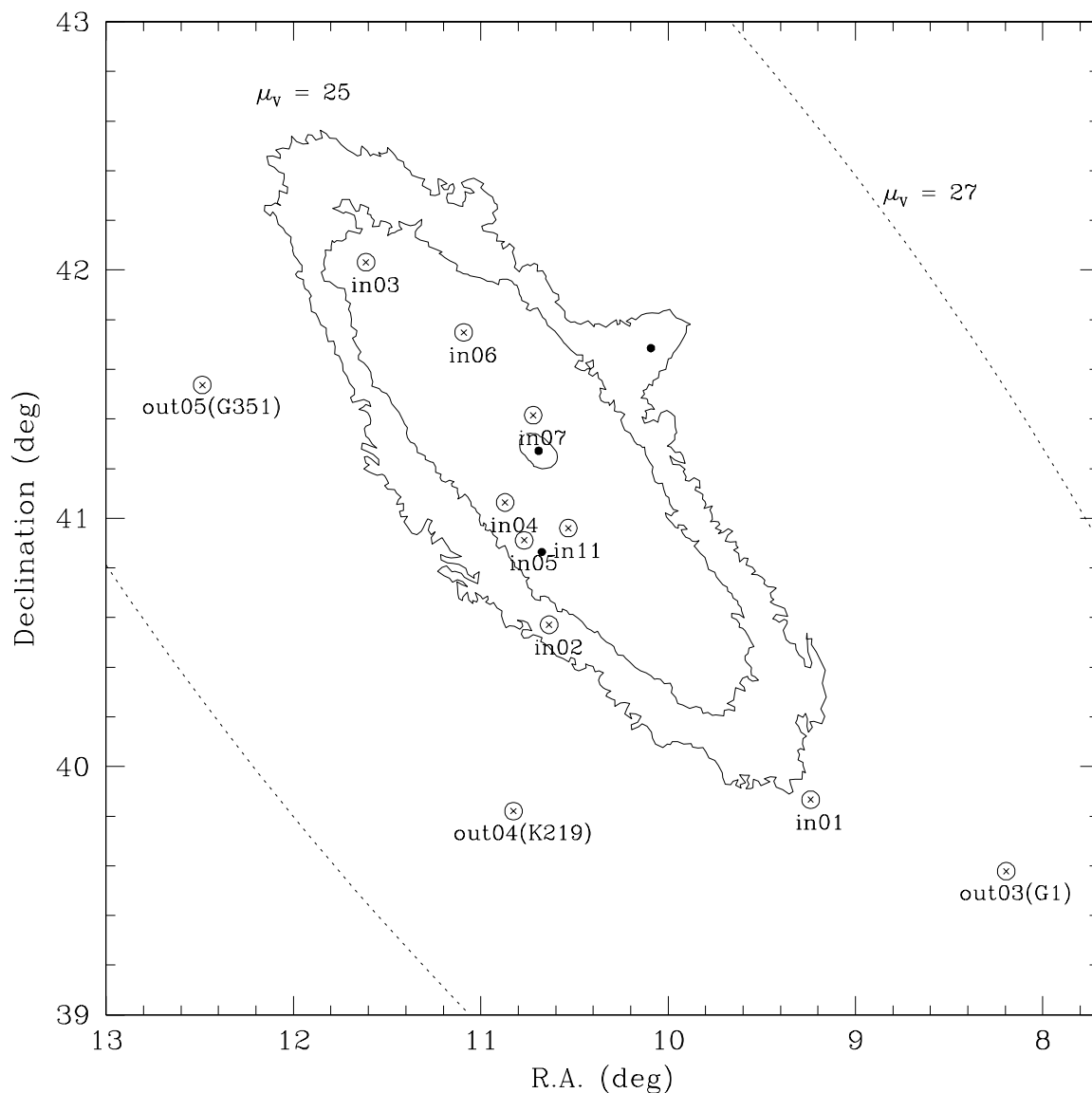


Fig. 1.— Program field locations are superimposed on M31 isophotes by Hodge & Kennicutt (1982), labelled by our internal ID. The three “out” fields happen to be globular cluster fields (with the cluster subtracted) and the cluster names are in parentheses. Isophotes for $\mu_B = 25$, 24, and near-nuclear 21 mag per square arcsec are shown. A rough guess for $\mu_B = 27$ is sketched. NGC 205 is marked by a dot located inside the $\mu = 25$ “finger” north of the M31 nucleus, and M32 is marked by a dot just to the left of the “in11” label.

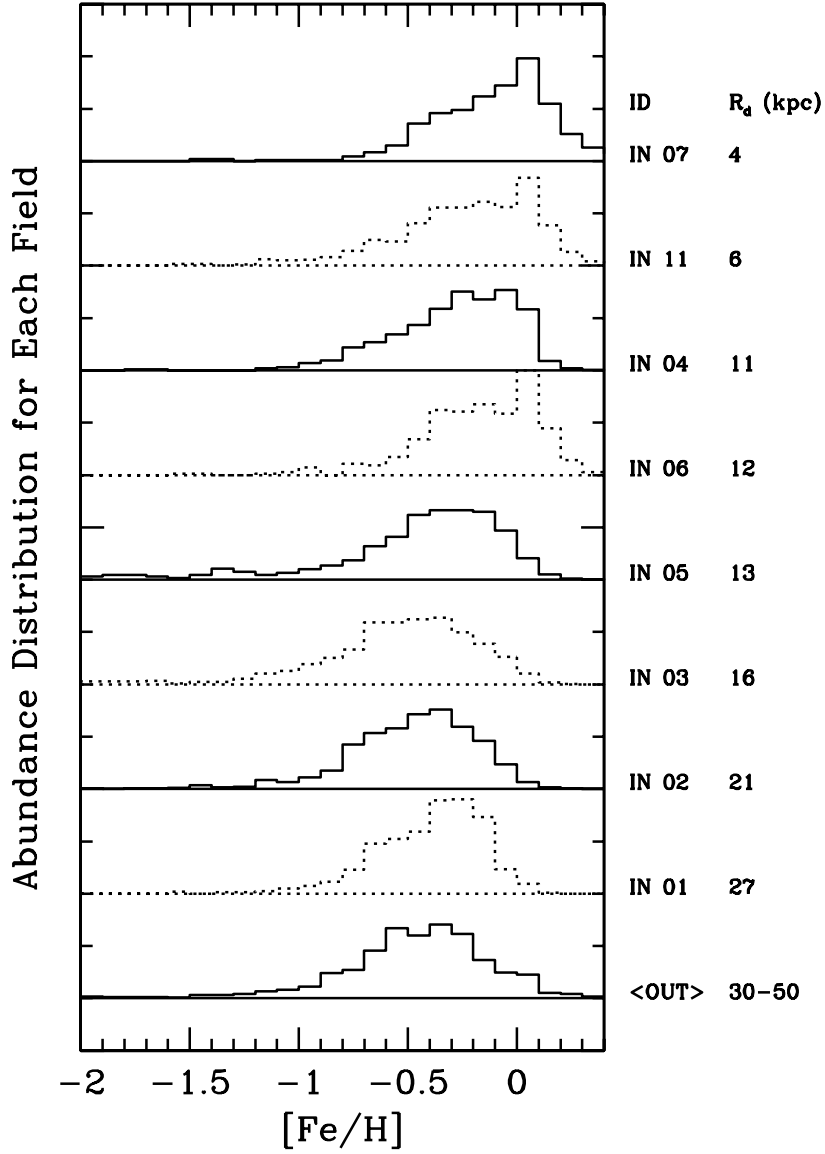


Fig. 2.— Derived abundance distributions for each field, except that the outer fields have been averaged. Each distribution has been normalised so that the numbers in all bins sums to one, bins are 0.1 dex wide, and each vertical tick mark is 0.1. Labels for each field appear to the right, along with the isophotal ellipse semi-major axis value associated with each field. A mild abundance gradient is clearly seen.

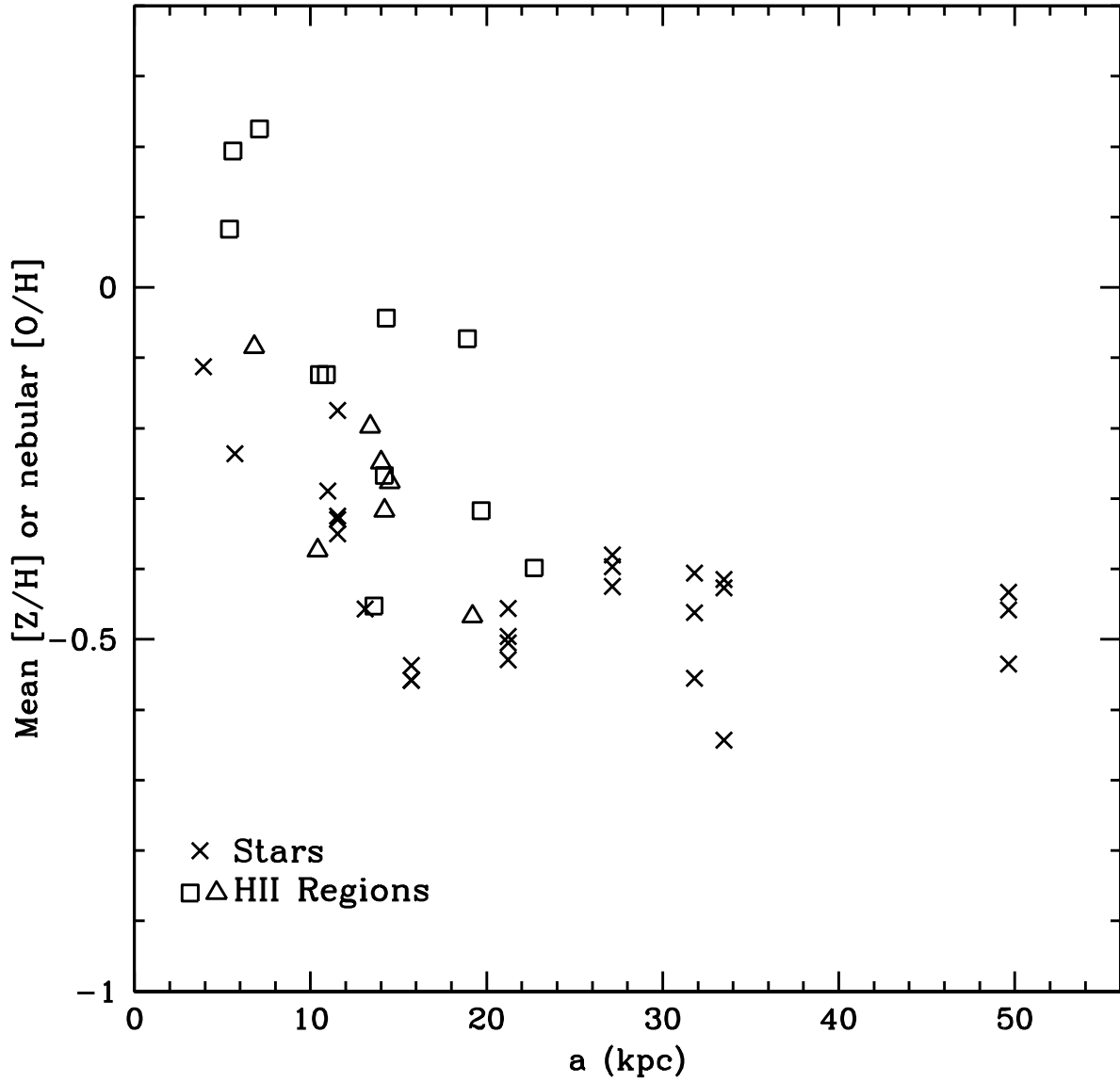


Fig. 3.— Median abundance for each field plotted as a function of galactocentric radius. Multiple points appearing at one radius indicate separate results for individual WFPC2 chips. Results from HII regions from Blair et al. (1982) and Dennefeld & Kunth (1981) are also shown as square and triangles, respectively.

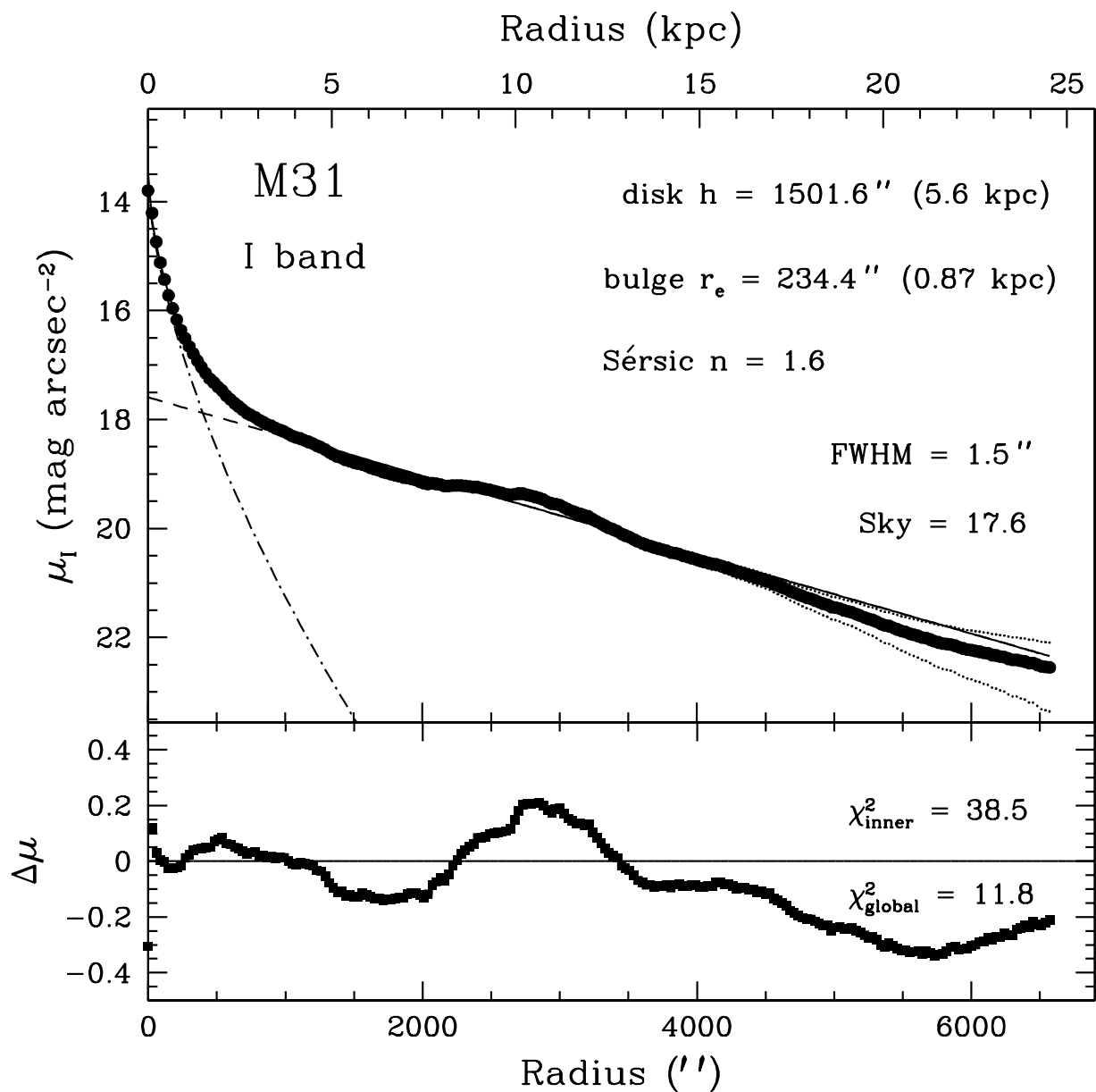


Fig. 4.— Azimuthally-averaged surface brightness profile from elliptical isophotal fits to the Choi et al. (2002) I-band image. The bulge light was fit with a Sérsic model of index $n = 1.6$, effective radius, $r_e = 234''.4$ ($=0.87$ kpc), and effective I-band surface brightness $\mu_e = 16.6$ mag arcsec 2 . The disk is described with an exponential profile of scale length $h = 1501''.6$ ($=5.6$ kpc) and a central I-band surface brightness $\mu_o = 17.6$ mag arcsec 2 . Residuals from the fit are shown in the lower panel. The χ^2 estimators and decomposition technique are fully described in MacArthur, Courteau, & Holtzman (2003).

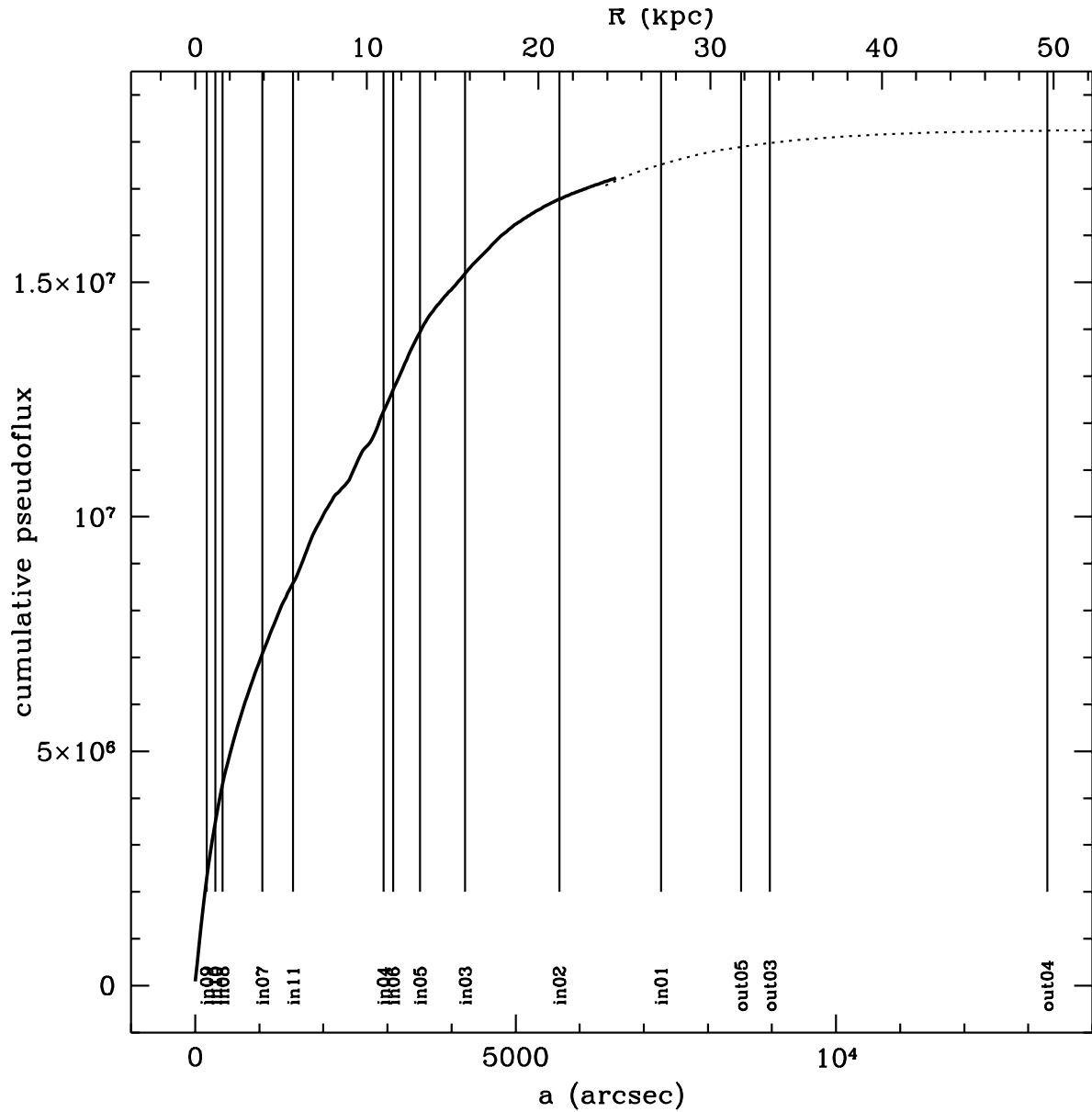


Fig. 5.— The measured cumulative surface brightness profile (inside 6400 arcsec) given in arbitrary flux units plus the assumed extrapolation (outside 6400 arcsec) are shown as a function of the semi-major axes of fitted elliptical isophotes. Locations of the target fields are also shown. Under the assumption of a circular disk geometry, galactocentric radii are given on the top scale assuming a distance of 770 kpc for M31. The three innermost fields were dropped from the analysis due to severe stellar crowding that prevented accurate photometry.

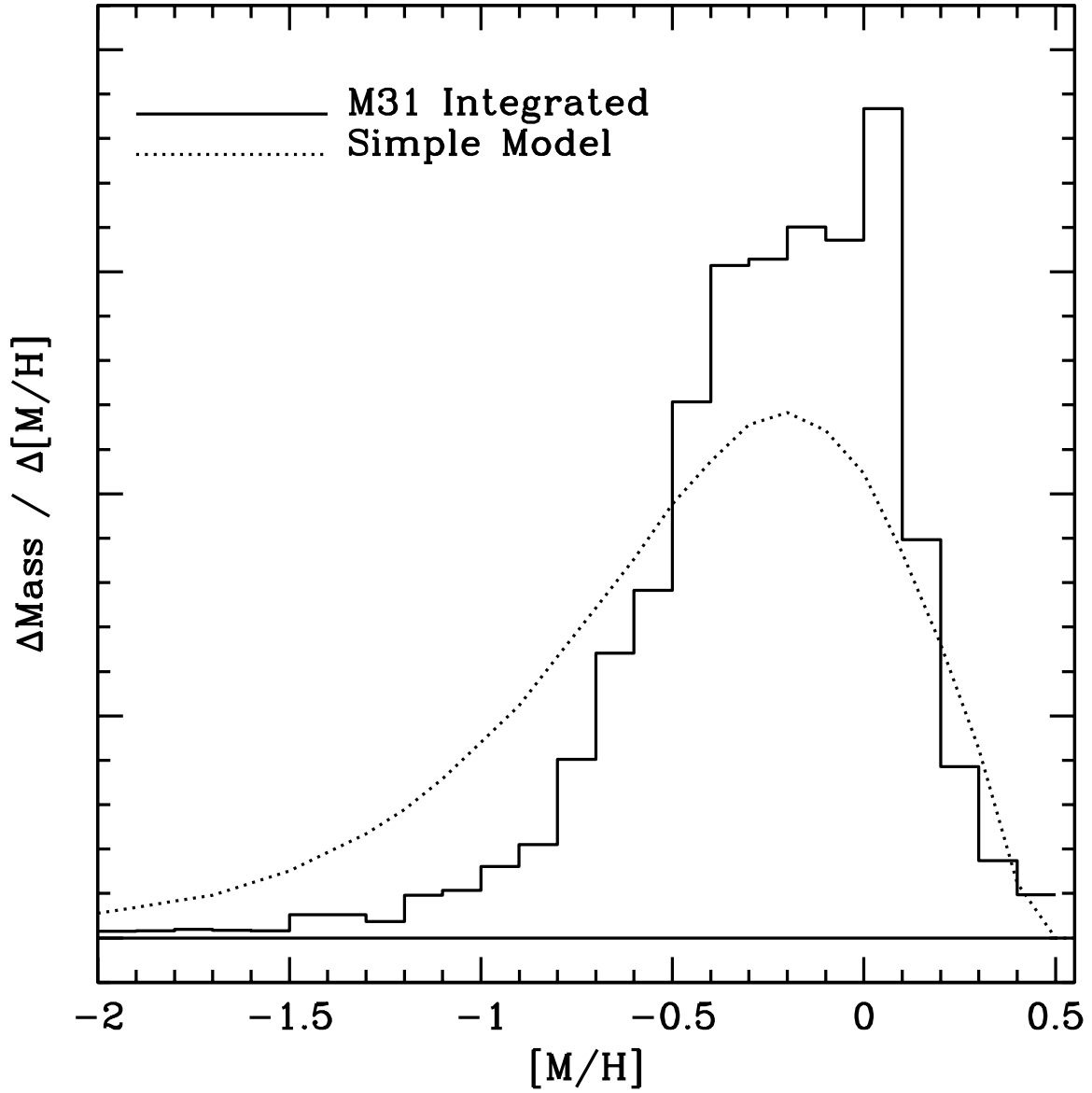


Fig. 6.— The global, weighted-sum M31 abundance distribution is compared to the Simple model with yield of $[\text{Fe}/\text{H}] = -0.2$ and a gas fraction of 2%.

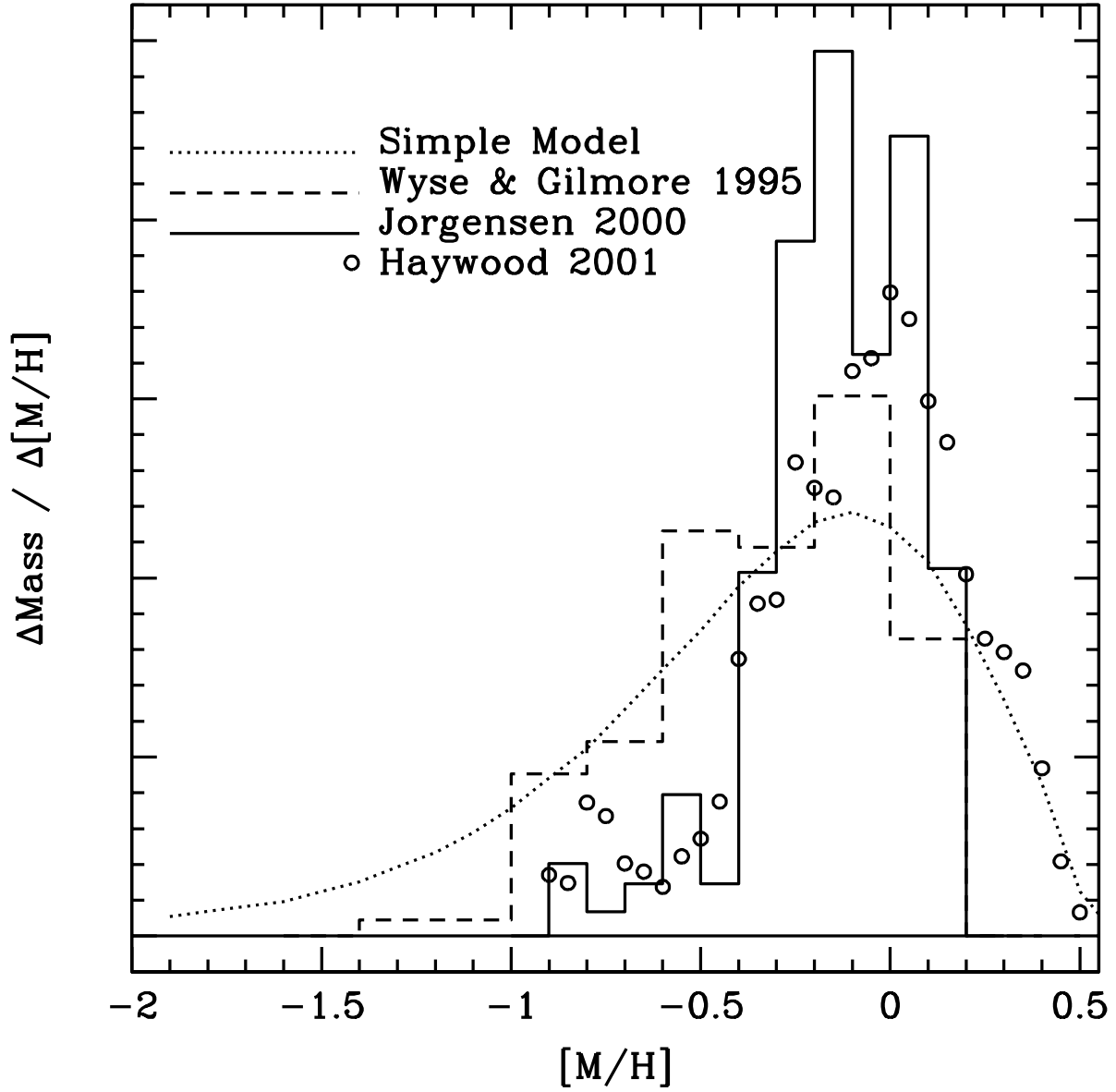


Fig. 7.— A Simple model with yield $[\text{Fe}/\text{H}] = -0.1$ and gas fraction of 2% is compared to three independent literature abundance distributions derived for the solar cylinder. The literature references are Wyse & Gilmore (1995), Jørgensen (2000), and Haywood (2001).

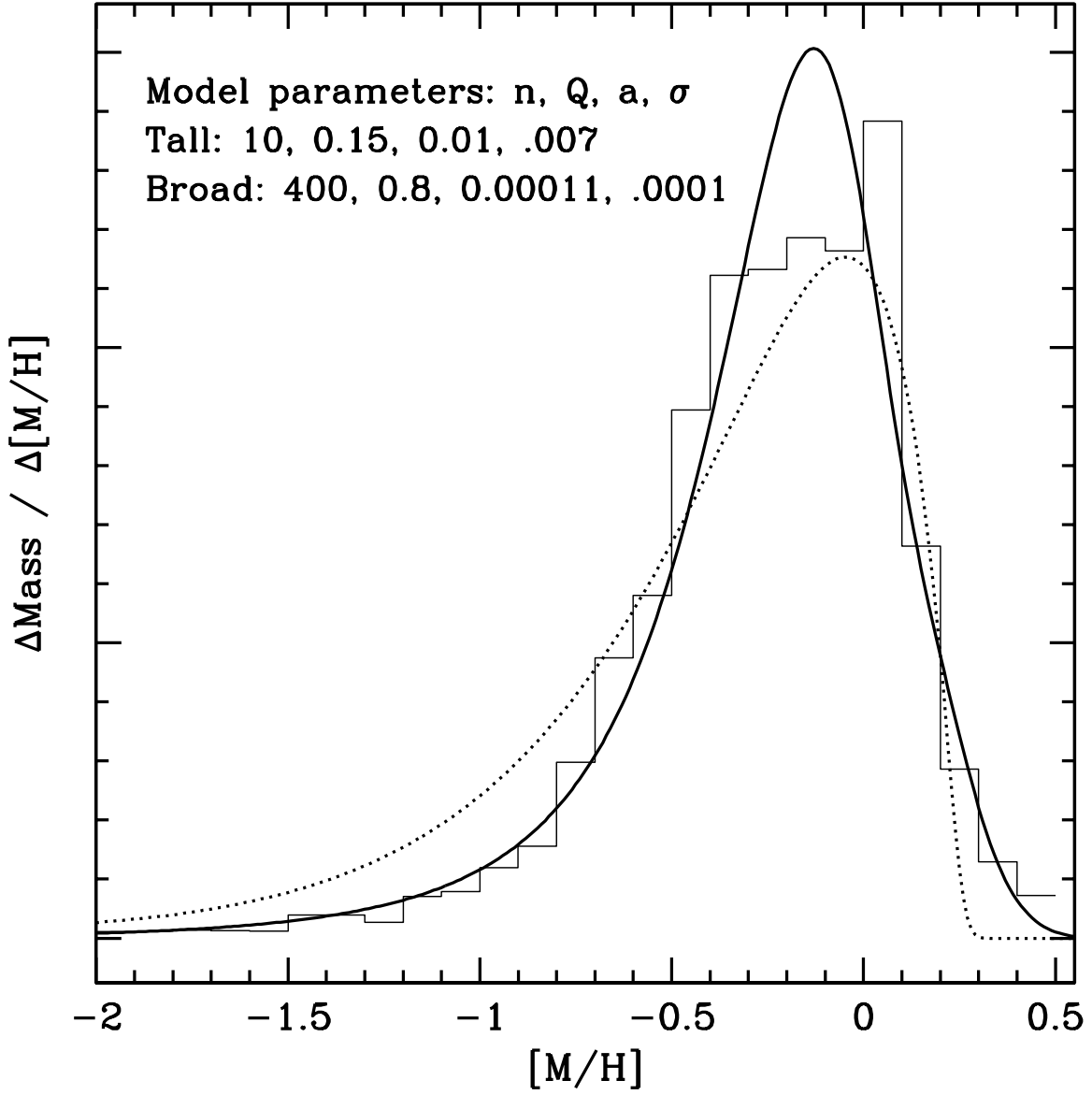


Fig. 8.— The M31 abundance distribution is compared to two inhomogeneous models computed using the formalism of Oey (2000) with $\mu = 0.02$ and other parameters as noted in the plot.

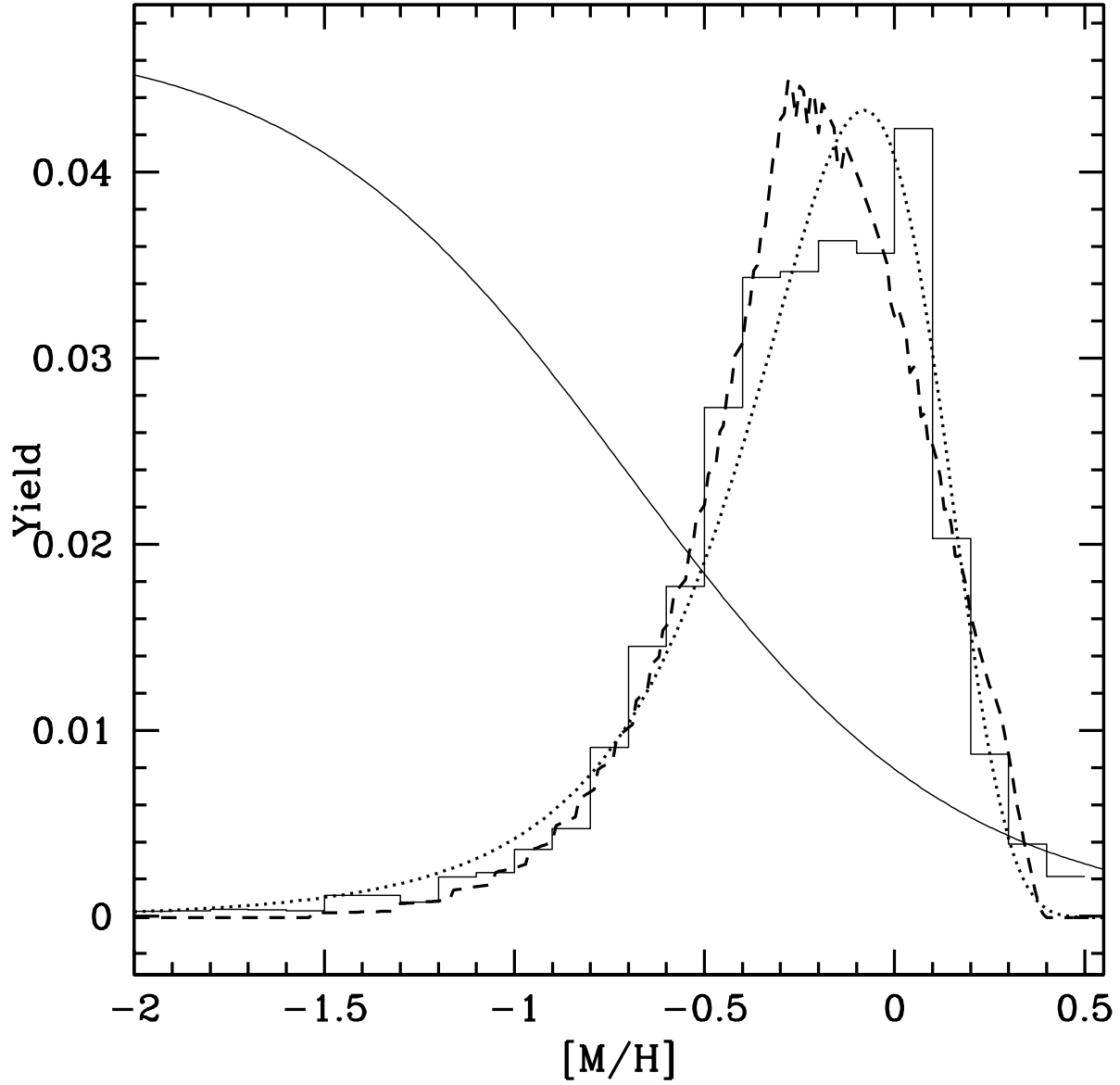


Fig. 9.— The M31 abundance distribution is compared to the rational decreasing yield model with $p_0 = 0.00019$ and $\epsilon = 0.004$ (dotted line). The thin line and the y-axis scale illustrate the yield p computed with these assumptions. The somewhat ragged dashed line is a Malinie et al. (1993) model with parameters as in their paper except that the initial metallicity is zero and the f parameter has been set to 0.075 so that the final gas fraction is 0.02.

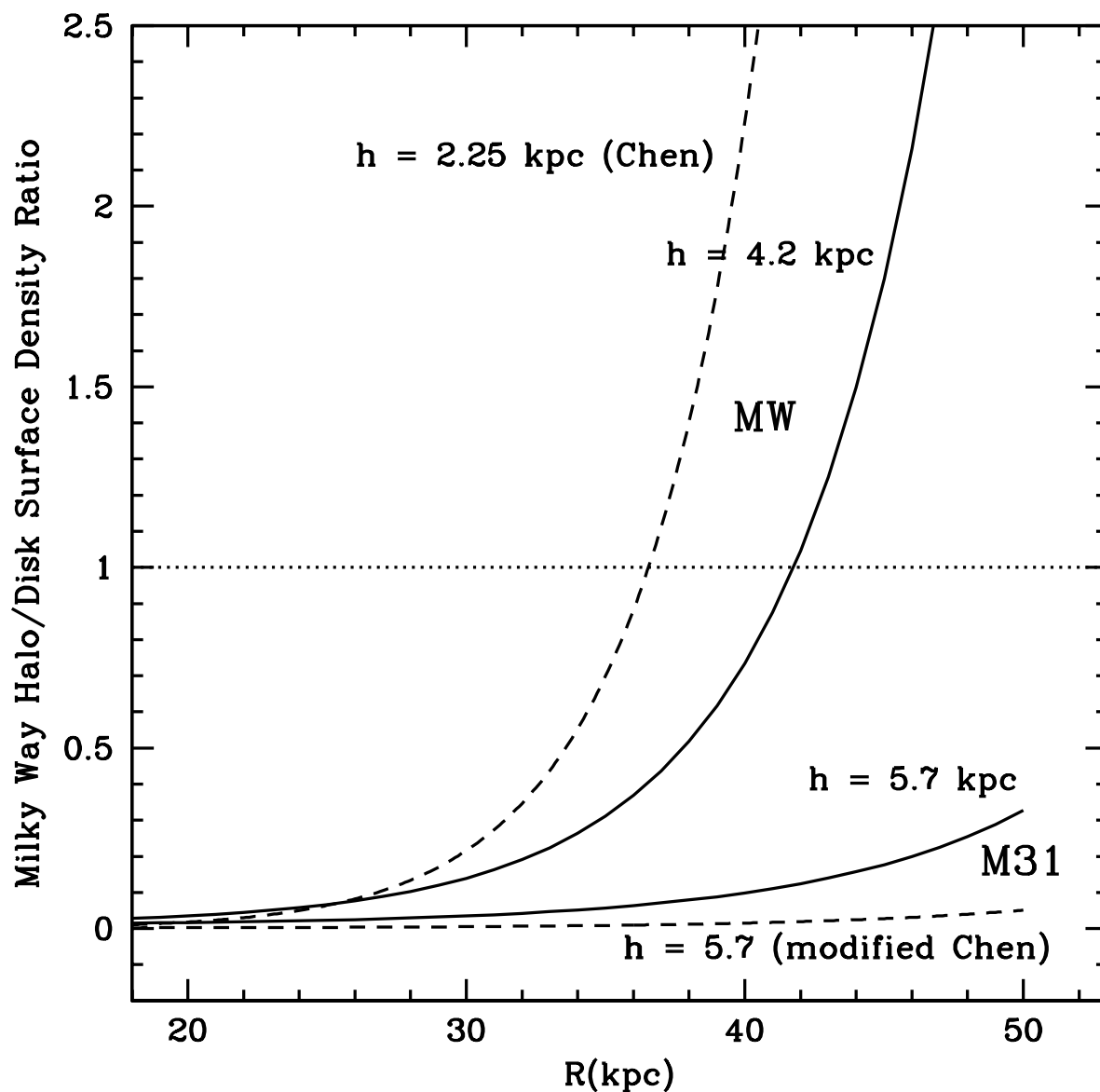


Fig. 10.— The ratio of halo to disk surface density (that is, projected on the x, y plane) for some models of the Milky Way. Values greater than one indicate that most stars seen by an observer distant from us and looking down on the disk would see halo stars, and values less than one indicate that disk stars dominate the light. The Chen et al. (2001) model has a scale length of 2.25 kpc, and a model based on Sandage (1987) plus van den Bergh (2000)'s preferred scale length of 4.2 kpc is also shown. The Milky Way in these models has a halo that becomes visible somewhere between 35 and 45 kpc. Both of these models are modified to emulate M31 by increasing the disk scale length to 5.7 kpc and doubling the density of the halo. The figure shows that, with a Milky Way-style halo, we should expect to see very few halo stars at 50 kpc from the center of M31.